International Journal of Engineering and Technology, 2 (1) (2013) 32-43
©Science Publishing Corporation
www.sciencepubco.com/index.php/IJET

Measurement of electron number density and electron temperature of laser-induced silver plasma

Muhammad Musadiq[a*], Nasir Amin[a], Yasir Jamil[a], Munawar Iqbal[b], M. Asif Naeem[a] and Hafiz Akif Shahzad[a]

[a]*Department of Physics, University of Agriculture, Faisalabad-38040, Pakistan*
[b]*Department of Chemistry and Biochemistry, University of Agriculture, Faisalabad-38040, Pakistan*
**Corresponding author E-mail: musadiquaf@gmail.com*

Abstract

Silver (Ag) plasma generated by second harmonics (532 nm) using Nd:YAG laser has been investigated at 17.6 mJ and 88.6 mJ energy level. The excitation temperature was determined from the Boltzmann plot method of the transition ($^3D_3 \rightarrow {}^3P_2$) at 243.779 nm, ($^2S_{1/2} \rightarrow {}^2P_{3/2}$) at 328.068 nm, ($^2S_{1/2} \rightarrow {}^2P_{1/2}$) at 338.289 nm, ($^2P_{1/2} \rightarrow {}^2D_{3/2}$) at 520.907 nm and ($^2P_{3/2} \rightarrow {}^2D_{5/2}$) at 546.550 nm, while the Stark Broadening (SB) method was used to measure the Electron Number Density (END) of $^2P_{3/2} \rightarrow {}^2S_{1/2}$ at 827.351 nm transition. The spatial behavior of the END and Electron Temperature (ET) was measured at ambient air pressures at different energy level and distance ranging from 0-4.5 mm form the target metal. The ET's were found to be varies from 17895 K to 10593 K, while END was found to be 2.229×10^{15} to 6.44×10^{14} cm^{-3} and 1.76×10^{16} to 1.893×10^{15} cm^{-3} for 17.6 mJ and 88.6 mJ energy, respectively. The relationship of END and ET found directly related to laser irradiance, while they were inverse to the distance from the target material surface to laser beam source.

Keywords: *Silver plasma; Electron temperature; Electron number density; Boltzmann plot; Laser-induced breakdown spectroscopy; Stark broadening*

1 Introduction

The Pulsed laser-induced plasmas (LIPs) has a intensive application in material processing, thin film deposition, environmental monitoring, biomedical studies, military safety usage, art restoration/conservation and metal analysis, which is being produced after laser irradiance on the surface of metals and is of a great interest since last few decades [1-11]. In LIPS method, a micro-plasma is produced in nanosecond when highly intense laser pulse interacts with a target material; resultantly vaporization take place and thus plasma produced expand along the path of distribution in the form of vapor plume. During the expansion process of vapor plume the Inverse Bremsstrahlung (IB) absorption also happened repeatedly which is considered as heat loss during plasma routine applications [12]. The wavelength, intensity of incident beam, energy absorption and transfer, duration of exposure, composition of targeted material as well as the environmental condition such as ambient air pressure and distance between the target and laser has a key role in the formation of plasma from irradiated material [13-14].

Laser-induced plasma spectroscopy (LIPS), also called laser-induced breakdown spectroscopy (LIBS) is based on the optical emission spectra for the elemental analysis. These days the LIBS technique has turns into an analytical technique to provide *in-situ*, remote, rapid and multi-elemental analysis of massive and traces sample in solid, liquid or even in gas phase [15-16]. The excitation and ionization temperature prevailing distribution of energy level and ionization equilibrium through Boltzmann equation and Saha equation, respectively are equal to ET describing the Maxwellian distribution of electron velocities and thus, one describes the plasma in local thermodynamic equilibrium (LTE) by a common temperature T, known as the plasma temperature. For this purpose, the Laser induced plasma (LIP) should be optically thin and under local thermodynamic equilibrium (LTE) state. Optical emission spectroscopy has recently attracted an attention worldwide for characterizing of materials based on laser induced plasma (LIP technique). The Boltzmann plot method is widely used for spectroscopic method to determine the temperature. For temperature determination, two or more atomic lines can also be used in the form of integrated line intensities ratio. For measuring the plasma END, N_e plasma spectroscopy based on either Stark broadening of spectral lines or the Saha-Boltzmann equation are being used [10, 13].

The END and ET can be determined from the emission spectrum of the plume [14]. Various researchers world wide have studied and reported effect of laser irradiation on Cu, Li, Zn, Al, Fe, Pb, Sn, Si and their alloy under ambient pressure, vacuum and using gases like argon and neon. They also studied the END and ET behavior at different laser harmonic, energy level and distances of target material from the laser irradiance by using ranges of spectroscopic methods [17-30].

From last few decades, due to diverse applications as well as ease of utilization, relative simplicity, low cost and highshot-rate capability of laser driven material has became a very important field and the description of material in the form of ET and END has added a substantial curiosity in recent years for the understanding and utilization of these complex matter in daily life. To best of our knowledge, laser irradiance and its effect on END and ET as function of energy and distance has not been reported yet for Ag, so, in the present work, we have investigated the Ag plasma formation behavior at 532 nm by Nd:YAG laser beam in ambient air. The optical emission has been spatially resolved by scanning the plume along the plasma expansion path. We have determined the ET using Boltzmann method and END by Stark line broadening method. Furthermore, we have also studied the variation in ET and END as a function of energy and distance of Ag target from laser source.

2 Experimental setup

We have used a laser system (Q-switched pulsed Nd: YAG laser, Quantel, Brilliant, repetition rate 10 Hz, pulse duration ≈ 4 ns, energy 180 mJ per pulse at 532 nm, The line width was 1.4 cm^{-1} at 532 nm). The laser pulse energy was varied by the flash lamp Q-switch delay through the laser controller and measured by an energy meter (Nova-Quantel P/niz01507). The laser beam was focused on the target using convex lens of 10 cm focal length. The sample was mounted on a 2-Dimensional sample stage, which was rotated to avoid the non-uniform pitting of the target. The distance between the focusing lens and the sample was kept less than the focal length of the lens to prevent any breakdown of the ambient air in front of the target. The spectra were obtained by averaging 3 data of single shot under identical experimental conditions. The radiation emitted by the plasma were collected by a fiber optics (high-OH, core diameter: 600 µm) having a collimating lens (0-450 field of view) placed at right angle to the direction of the laser beam. This optical fiber was connected with the HR 4000 spectrometer (Ocean optics Inc) to measure the plasma emission. The emission signal was corrected by subtracting the dark signal of the detector through the OOI software. The pulse energy of the Nd:YAG laser was varied through the remote control of laser [14]. The data acquired by the spectrometer was stored on a PC through the OOI HR4000 software for subsequent analysis and the END was measured in laser produced plasma by utilizing the Stark broadening method, while ET by Boltzmann method as precisely described by Sherbini *et al.* [31].

3 Results and discussion

The emission spectra of the plasma produced at the Ag surface were recorded from 0 to 4.5 mm distance along the path of spreading out of the plume generated by Q-switched Nd:YAG laser irradiance. The second harmonic 532 nm of 17.6 mJ and 88.6 mJ energy was targeted on Ag surface in ambient air and the results of the emission spectrum of Ag ranging form spectral region (243.77 to 827.35 nm) are shown in fig. 1 (a-d), fig. 2 (a-f), fig. 3 (a-d) and fig. 4 (a-f). It is very clear that the spectral regions are separated well as result of emission either from neutral Ag atoms or ions. According to Grein [32] the spectral region between 200-260 nm is associated with Ag (I), while the region between 260-315 nm showed both Ag (I) and Ag (II) lines and the region between 360-520 nm also showed the mixed lines of neutral and ionic Ag atom. We have used the spectral lines signal at 241.318, 243.77, 328.06, 338.28, 520.90, 546.55, 786.77 and 827.35 nm and identity were done using the NBS (NIST) data-base system as reported by Fuhr and Wiese [33]. It has been noted that the plasma generate very shortly and long-drawn-out due to shock waves generation at the surface of the target Ag. It is well known that the plasma usually transmits as a supersonic absorption wave against the incident laser beam during breakdown process in the longitudinal and lateral dimensions to the target and independent of the angle of incidence of the laser beam. The identification of these transitions parallel to the configurations states are given in table 1, along with their transition probabilities (Fig. 7). The spectra having well resolved doublet structure from a number of excited levels decaying to common lower levels is of more interest and spectroscopically more informative regarding the END and plasma ET. The Ag (II) at lower wavelength belongs to the $4d^9\,5p\ ^3F_3 \rightarrow 4d^9 5s\ ^3D_2$ and $4d^9 5p\ ^3P_2 \rightarrow 4d^9 5s\ ^3D_3$ transition. Figure 7 depicts the schematic diagram of de-excitation channels responsible for the emission lines of the ionized Ag, showing well-resolved multiplet level from a number of excited levels decaying to common lower levels. The density of the emitted electron was found much high near the surface of the target material, because signal response was higher at lower distance as compared to longer ones (Fig 1, 2 and 3).

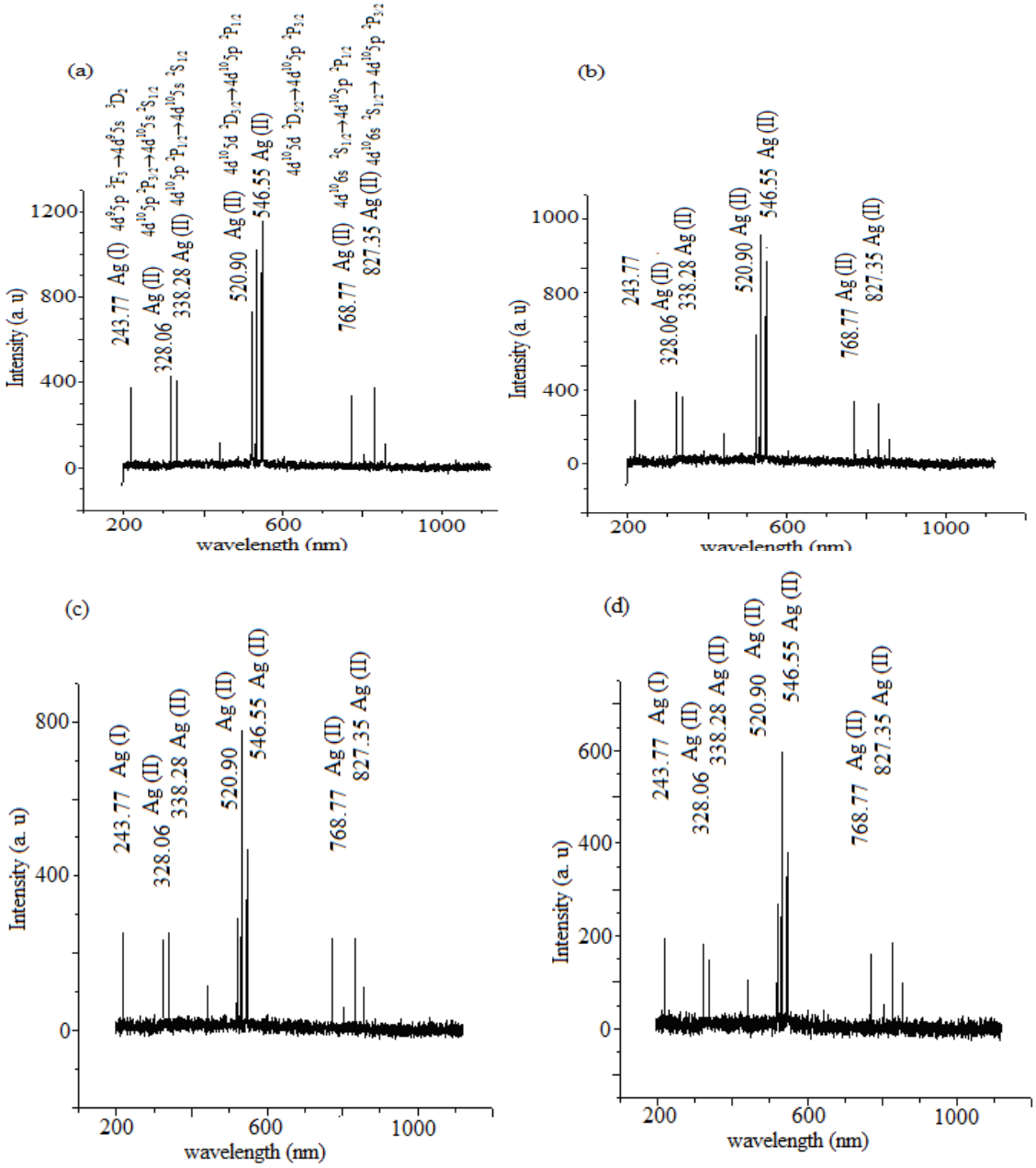

Fig. 1: The emission spectrum generated by the 532 nm laser showing the Ag spectral lines at 17.6 mJ energy level (a) 0 mm distance, (b) 0.5 mm, (c) 1 mm, (d) 1.5 mm.

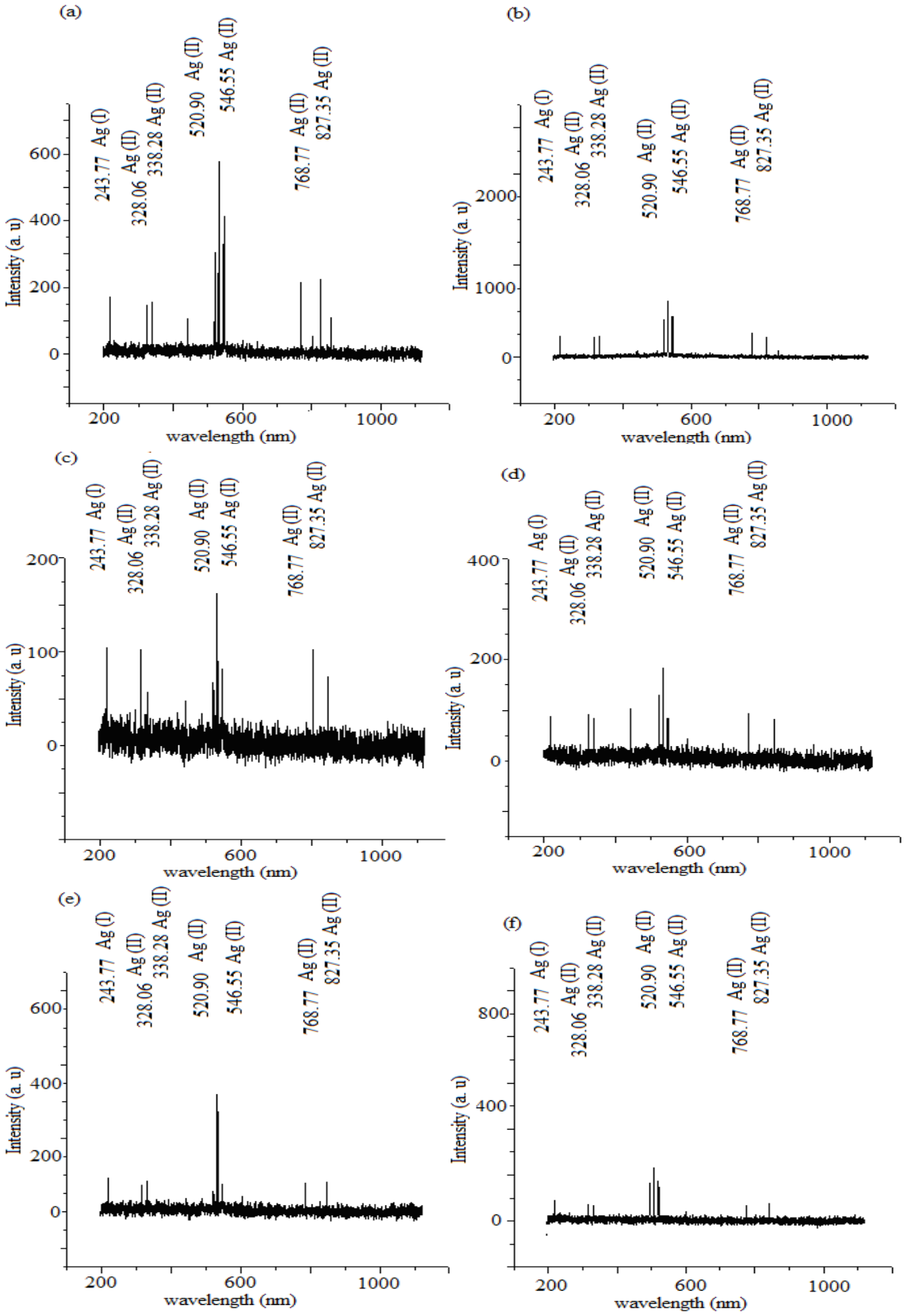

Fig. 2: The emission spectrum generated by the 532 nm laser showing the Ag spectral lines at 17.6 mJ energy level (a) 2 mm distance, (b) 2.5 mm, (c) 3 mm, (d) 3.5 mm, (e) 4 mm (f) 4.5 mm.

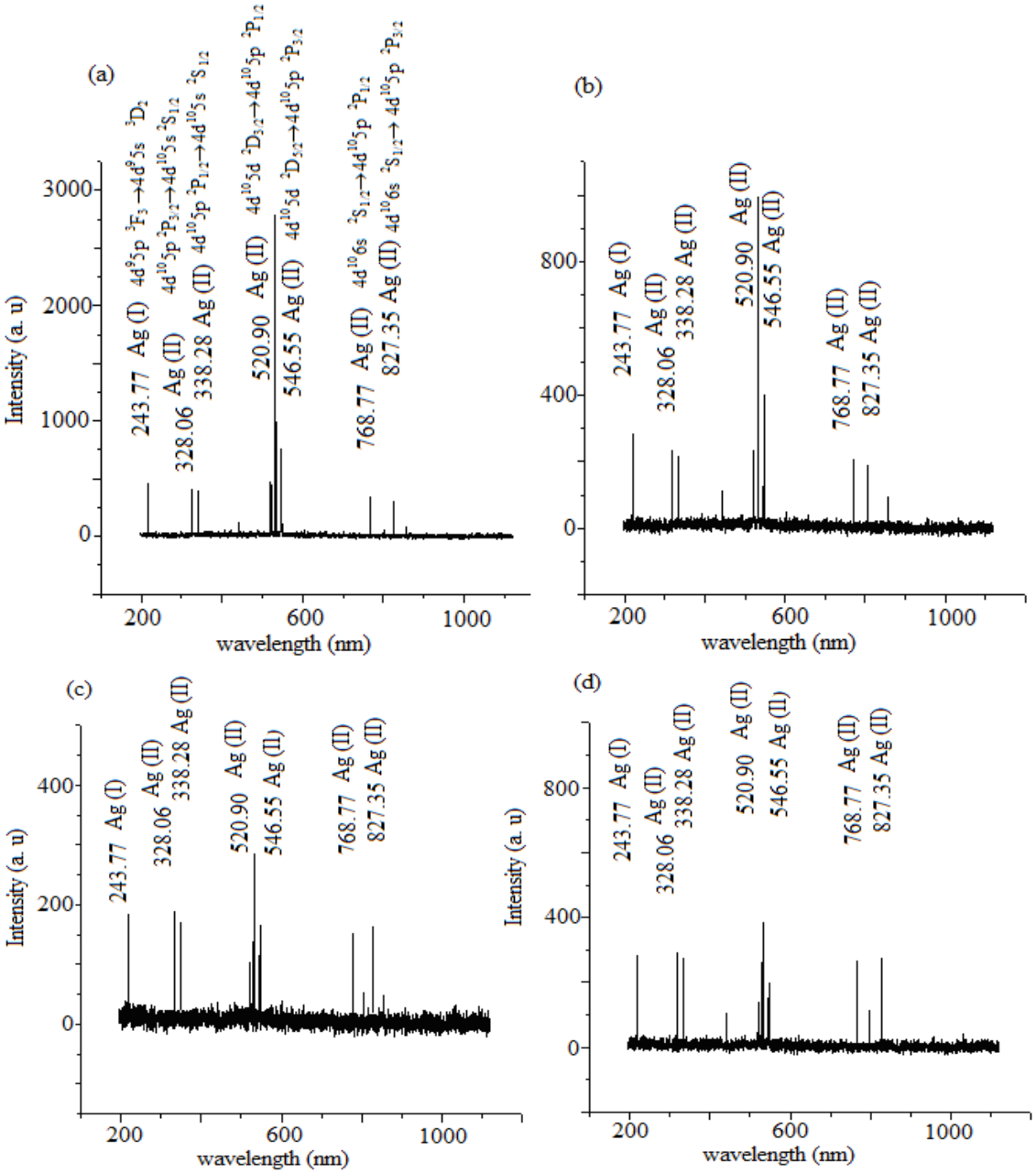

Fig. 3: The emission spectrum generated by the 532 nm laser showing the Ag spectral lines at 88.6 mJ energy level (a) 0 mm distance, (b) 0.5 mm, (c) 1 mm, (d) 1.5 mm.

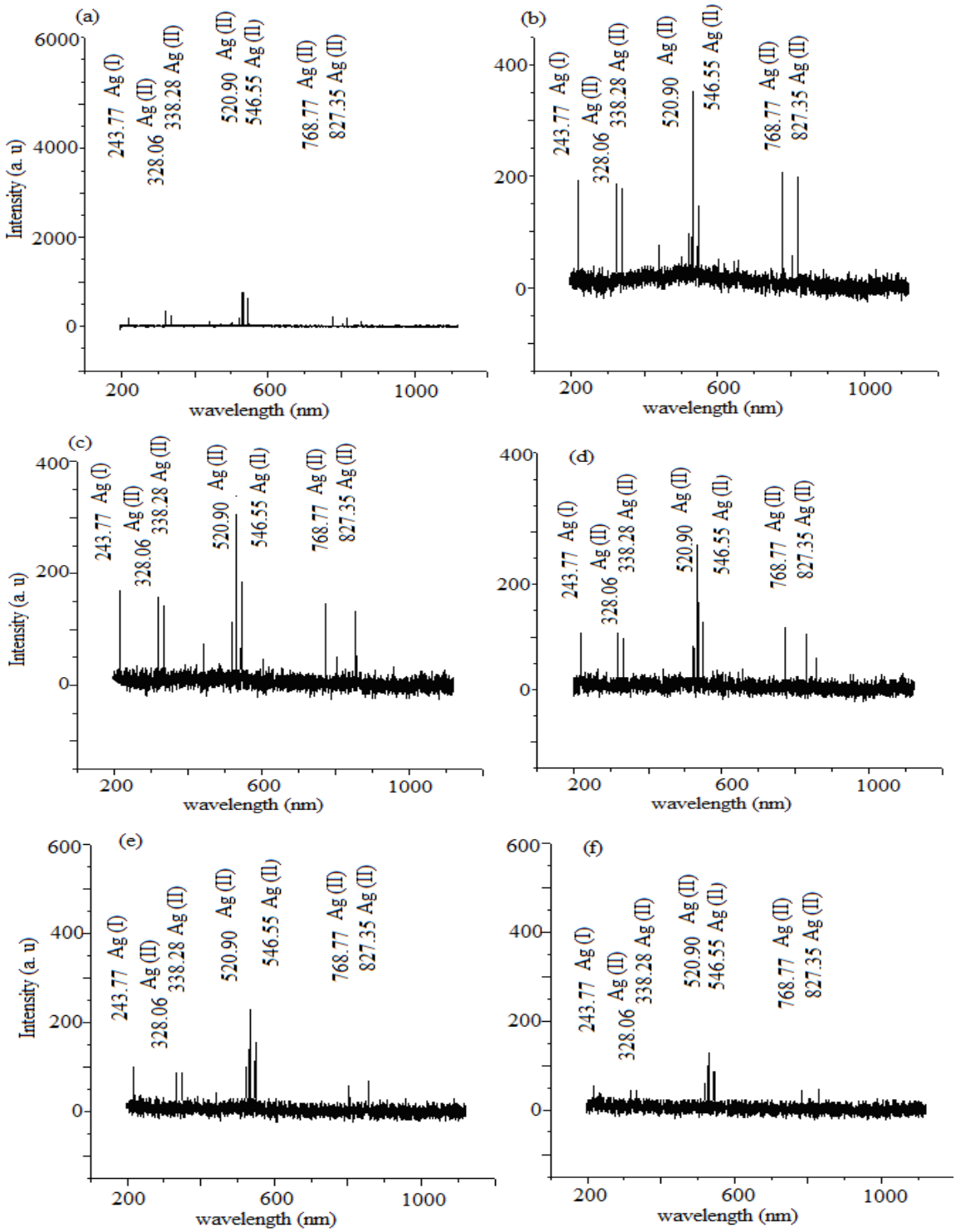

Fig 4: The emission spectrum generated by the 532 nm laser showing the Ag spectral lines at 88.6 mJ energy level (a) 2 mm distance, (b) 2.5 mm, (c) 3 mm, (d) 3.5 mm, (e) 4 mm (f) 4.5 mm.

3.1 Electron temperature and electron number density (END and ET)

The ET has been evaluated using the ratio of the relative intensities of spectral lines as described by [14].

$$v = \left(\frac{E_i - E_j}{h} \right) \tag{1}$$

$$\frac{dN_{i\to j}}{dt} = A_{ij} N_i \tag{2}$$

In this equation N_i (unit volume of emitting gas contain) atoms in an excited state of energy E_i above the ground state and a number of them ($dN_{i\to j}$) per unit time undergo spontaneous transitions to lower state of energy E_j through emission of an equal number of photons of frequency. The number $dN_{i\to j}$ is proportional to the population N_i of the initial state

$$I = A_{ij}\, h\nu N_i \tag{3}$$

The emission intensity I of a line is the energy given out per unit time and is equal to the product of the number $dN_{i\to j}$ of produced photons by the energy $h\nu$ of each photon.
According to Boltzmann method, when thermal equilibrium is attained at absolute temperature T, the average number of particles of a given species n_i and n_j with energies E_i and E_j are in the ratio as:

$$\frac{n_i}{n_j} = \exp\left(-\left(\frac{E_i - E_j}{kT}\right)\right) \tag{4}$$

The oldest method for the determination of ET in LTE plasma is based on the fact that densities in various excited states are proportional to the statistical weight with the exponential of negative ratio of excitation energy and the thermal energy kT;

$$N = g \exp\left(-\frac{\Delta E}{kT}\right) \tag{5}$$

Where g = 2J + 1 (statistical weight).

$$\frac{I}{gAh\nu} = \exp\left(-\frac{\Delta E}{kT}\right) \tag{6}$$

Taking ℓn of both sides

$$\ln\left(\frac{\lambda I}{gAhc}\right) = -\frac{\Delta E}{kT} \tag{7}$$

$$kT = -\frac{\Delta E}{\ln\left(\frac{\lambda I}{ghcA}\right)} \tag{8}$$

The ET was calculated from the slope (-1/kT) from the straight line graph ln(λI/hcgA) versus E. It is well known that END and ET are interdependent and validity of the Boltzmann relationship needs LTE condition, because in this condition it is probable to find a temperature which may vary from place to place, fits the Boltzmann-Saha distribution and also Maxwell distribution for velocities of electron. For LTE condition the collision process is of a more interest then radiative process.
Various spectroscopic factor such as statistical weight ($g_{(ki)}$), transition probability (A) wavelength (λ) and energies (E) are given in Table 1 and 2, taken from [32-33] and for calculation of plasma ET and END, the lines appeared at 243.779 nm, 328.068 nm, 338.289 nm, 520.907 nm, 546.550 nm, 768.777 nm, 827.351 nm being used in present study.
The ET was calculated from a straight line graph (ln($\frac{\lambda I}{hcgA}$) versus distance) having slope (-1/ KT) and excitation temperature was taken from the Boltzmann plot, while the END was calculated by Stark broadening method using different spectral lines [14].

Table 1: Spectroscopic parameters of the observed Ag (I) lines

Wavelength λ (nm)	Transitions	Statistical weight		Transition probability A (s^{-1})	Upper level Energy E_k (cm^{-1})
		g_i	g_k		
328.068	$4d^{10}\ 5p\ ^2P_{3/2} \rightarrow 4d^{10}\ 5s\ ^2S_{1/2}$	2	4	1.4×10^8	30472.703
338.289	$4d^{10}5p\ ^2P_{1/2} \rightarrow 4\ d^{10}5s\ ^2S_{1/2}$	2	2	1.3×10^8	29552.061
520.907	$4\ d^{10}5d\ ^2D_{3/2} \rightarrow 4d^{10}5p\ ^2P_{1/2}$	2	4	7.5×10^7	48743.969
546.550	$4d^{10}5d\ ^2D_{5/2} \rightarrow 4d^{10}5p\ ^2P_{3/2}$	4	6	8.6×10^7	48764.219
768.77	$4d^{10}6s\ ^2S_{1/2} \rightarrow 4d^{10}5p\ ^2P_{1/2}$	2	2		42556.152
827.351	$4d^{10}6s\ ^2S_{1/2} \rightarrow 4d^{10}5p\ ^2P_{3/2}$	4	2		42556.152

Table 2: Spectroscopic parameters of the observed Ag (II) lines

Wavelength λ (nm)	Transitions	Statistical weight		Transition probability A (s^{-1})	Upper level Energy E_k (cm^{-1})
		g_i	g_k		
241.318	$4d^9\ 5p\ ^3F_3 \rightarrow 4d^9 5s\ ^3D_2$	5	7	2.21×10^8	82171.697
243.779	$4d^9 5p\ ^3P_2 \rightarrow 4d^9 5s\ ^3D_3$	7	5	2.88×10^8	80176.425

The ET behavior has been studied as a function of distance from 0-4.5 mm of target surface by 532 nm wavelength of laser irradiance (Fig 5). The ET close to the target surface was recorded very high (17895 K), decreased to 9523 K as distance increases to 4.5 mm form laser beam source to Ag surface. This difference between 17.6 and 88.6 mJ energy level was found to be significant (*P<0.05*). The ET near Ag surface as well as at 4.5 mm distance was found higher for 88.6 mJ laser irradiance verses 17.6 mJ energy. The temperature at 0 mm distance was found to be 17895 K and 15997 K, respectively for 86.6 mJ and 17.6 mJ, while it was 10593 K and 9523 K at 4.5 mm distance. As a function of distance, the difference in the ET from the target surface for the plasma formed by 532 nm laser irradiance is given in fig. 5 and it is found that ET has positive correlation with energy which is surely due to higher laser energy transfer at specific energy level. The high ET near the Ag surface might be attributed to take up more radiant energy during the laser pulse interaction. According to Rashid et al. [34] the higher value of the ET near the surface is due to the absorption of laser radiation by means of electrons via the IB absorption process and decrease in the ET is due to the fact that the thermal energy is rapidly converted into KE when the plasma attained the maximum expansion velocities, causing the temperature to drop as a result of plasma expansion. Ying et al. [35] also reported similar results for ArF excimer laser irradiance in which the ET varied from 9280 to 8120 K at a distance ranging from 0 to 17 mm from the surface of the target and Lindner et al. [36] also reported similar results of laser-particle interaction in laser induced breakdown spectroscopy and laser ablation inductively coupled plasma spectrometry in case of ET.
The minimum END required for the LTE condition was estimated from the equation 9 [12, 32, 37].

$$Ne \geq 1.6 \times 10^{12}\ T1/2\ (\Delta E)^3 \tag{9}$$

In this equation, T (K) is the ET and ΔE (eV) is the energy difference between the states. The END "Ne" can also be calculated from the width of a spectral line. It is observed that the width of the lines increases with the increase in laser energy. In plasma, the spectral lines are normally broad and the main sources of the line broadening is doppler broadening and Stark broadening [14]. The Doppler width can be estimated from the equation 10 [38].

$$\Delta\lambda = \lambda\sqrt{\frac{8kT\ln 2}{Mc^2}} \tag{10}$$

The Stark broadening line width $\Delta\lambda_{1/2}$ (FWHM) can be calculated using the equation 11 as:

$$\Delta\lambda_{1/2(Stark)} = 2\omega\left(\frac{N_e}{10^{16}}\right) + 3.5A\left(\frac{N_e}{10^{16}}\right)^{1/4}\left[1-\frac{3}{4}N_D^{-1/3}\right]\omega\left(\frac{N_e}{10^{16}}\right) \quad (11)$$

In equation 11, the ω, A, Ne and N_D represents the electron impact width parameter, ion broadening parameter, END and number of particles in the Debye sphere, respectively. The first part of equation 11 represents the broadening due to the electron contribution, while the second part represents the ion broadening. Since the contribution of the ionic broadening is usually very small, it can be neglected and the equation 11 condensed to equation 12 as:

$$\Delta\lambda_{1/2} = 2\omega\left(\frac{N_e}{10^{16}}\right) \quad (12)$$

From equation 12, the END was determined of plasma produced by the 532 nm laser at two energy levels (17.6mJ and 88.6 mJ) and is given in figures 6. In this spatial behavior of the Ag plasma, the END were found to be ranged from 2.229×10^{15} to 6.44×10^{14} cm^{-3} and 1.76×10^{16} to 1.893×10^{15} cm^{-3} as a function of distance along the direction of plasma expansion. It is evident that the END has a maximum value region near the surface and deceasing trend was found along the path of expansion of the plasma. According to Rashid et al. [34] the recombination process causes a decrease in the END in the expanded part of the plasma.

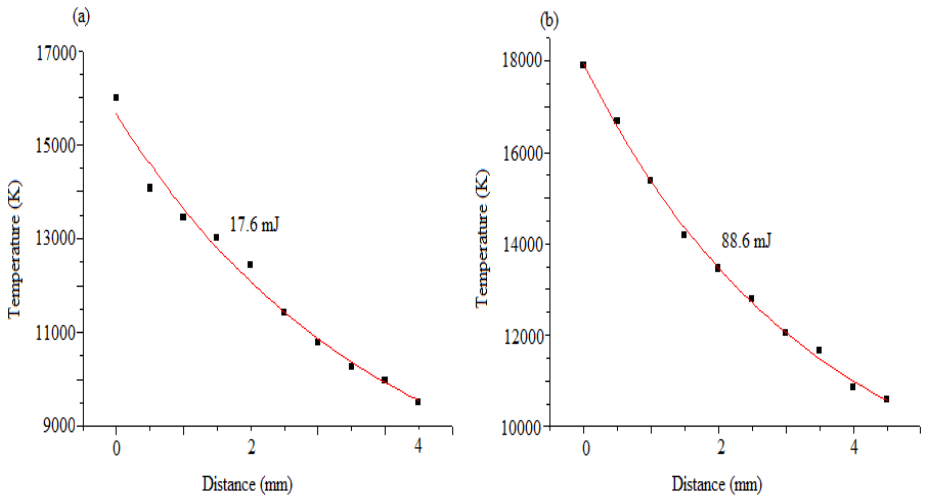

Fig 5: Effect on electron temperature and electron number density along the direction of propagation of the plume at 532 nm.

The END observed higher at lower wavelength of laser irradiance which indicates that the mass ablation rate may be higher for the shorter wavelength. This is similar as reported [36] that mass ablation rate increases as the laser irradiance wavelength is decreased. Similar behavior of the END was also reported by [39]. The behavior of the END and ET for different values of laser irradiance studied in the present work and is given in fig. 5 and 6 and it is noted that the ET and END increases by laser irradiance at 88.6 mJ verses 17.6 mJ, but as the distance increases, the ET and END was decreased constantly. The ET varies from 17895 K and 15997 K, whereas the END ranges from 1.893×10^{15} cm^{-3} to 6.44×10^{14} cm^{-3}. According to [14, 34] such behavior of the ET and END is attributed to the absorption or reflection of the laser energy by the plasma during formation which depends on frequency. They have reported the lower plasma frequency as compared to laser frequency, considered an energy loss in practically applications. They also indicated that by increasing the laser irradiance more excited species, ions and free electrons are produced and laser pulse interacts with these species, resulting in further heating and ionization. Resultantly, more consumption of the incoming laser energy can take place. It is well known that during plasma formation, there are two main processes of absorption, namely inverse bremsstrahlung absorption (IB) and photoionization. Shaikh et al. [14] and Rashid et al. [34] calculated the IB process and proved that the IB process is more efficient due to the λ^3 dependence of the electron-ion IB process. Our results regarding the ET and END are in line with various researches e.g. Abdellatif and Imam [26] diagnosed a Al plasma produced by A Q-switched Nd:YAG laser at wavelengths 1064, 532 and 355 nm with 500, 100 and 60 mJ energies, respectively and pulse duration of 7 ns with repetition rate of 1 Hz and measured the spatial behavior of ET using the Boltzmann plot method for the Al (II) lines and the END by Stark broadening method. The maximum attainable value of the ET was found at specific distance from the target surface, while the END accomplishes its

highest value close to the surface. Unnikrishnan et al. [29] studied the Cu plasma characteristics at 355 nm pulsed Nd:YAG laser with a pulse duration of 6 ns at atmospheric pressure. The ET and END characterizing the plasma were measured by time-resolved spectroscopy of neutral atom and ion line emissions in the time window of 300-2000 ns. He measured the ET via Boltzmann plot method and the END by Saha-Boltzmann technique. The ET and END was measured as a function of time relating to the onset of the laser pulse and found that the plasma should be optically thin and also LTE condition is necessary for LIBS analysis of samples and deduced from the temporal evolution of the intensity ratio of two Cu (I) lines. Similarly, Wu et al. [41] reported the optical emission spectroscopy on the laser-induced Cu plasma generated in the process of laser-driven flyer. They were also recorded copper plasma in the air to understand the disparity between the plasma with the confinement and without the confinement and found that under the same laser fluence, the plasma exists a longer time with the confinement. The time-resolved ET and END with the confinement were higher than those with no confinement. Shaikh et al. [14] studied the Zn plasma produced in air by the three harmonics of a Q-switched pulsed Nd :YAG laser at 1064, 532 and 355 nm and ET was determined from the intensity ratio of the transitions (4s4d $3D_3 \rightarrow$ 4s4p $3P_2$) at 334.5 nm and (4s5s $3S_1 \rightarrow$ 4s4p $3P_2$) at 481.0 nm of neutral Zn, while the END was measured by Stark broadening method of the transition (4s4d $3D_3 \rightarrow$ 4s4p $3P_2$) at 334.5 nm. They concluded that the ET and END decreases as the distance from the target surface increases and increases with an increase in the laser energy. Aguilera et al. [28] measured the intensity, temperature and electron density distribution of LIPs by emission spectroscopy with two dimensional spatial resolution and temporal resolution in Fe at different pressures. The temperature distribution has shown a slight difference between the intensity distribution of two Fe emission lines with high temperature distribution and also the electron density distribution showed similar features as that of temperature distribution. The characteristics of both parameters showed significant changes in different pressures. Rashid et al. [34] reported the Cu plasma parameters generated by the fundamental, second and third harmonics of a Nd:YAG laser. The 3 d^9 4s5s $2D_{3/2} \rightarrow$3 d^9 4s4p $2F_{5/2}$ at 464.25 nm, 4p $2P_{3/2} \rightarrow 3d^9$ 4s $2D_{5/2}$ at 510.55 nm, 4d 2 $D_{3/2} \rightarrow$4p $2P_{1/2}$ at 515.32 nm 4d 2 $D_{5/2} \rightarrow$4p $2P_{3/2}$ at 521.82 nm and 4p 2 $P_{3/2} \rightarrow 3d^9$ 4s $2D_{3/2}$ at 570.02 nm transitions was used to measure the ET. The spatial behavior of the temperature and END were examined at different ambient air pressures and under varied laser irradiance. The ET and END were found to be in the range from 14700 to 13600 K and 2.1×10^{16} to 1.78×10^{16} cm^{-3} for the 1064 nm laser, from 14200 to 12800 K and 2.2×10^{16} to 1.8×10^{16} cm^{-3} for the 532 nm laser and from 14100 to 12500 K and 2.4×10^{16} to 1.9×10^{16} cm^{-3} for the 355 nm laser irradiance. Ma *et al.* [6] studied the expansion of a vapor plume ablated from an Al target into an argon gas at atmospheric pressure using time and space-resolved emission spectroscopy and found plasma core with quite uniform distributions in electron density, temperature and electron number densities. Aragón and Aguilera [22] measured the local electron density in laser-induced plasma of three reference lines (Hα, Fe I and Si II) in air using a Nd:YAG laser and observed that the three lines was emitted from different regions of the plasma. Prokisch et al. [25] determined the electron number densities and temperatures for modified MPT and the END and ET were found in the range of 10^{20} m^3 to 10^{21} m^3 and of 16000-18000 K, respectively. By increasing the power from 80 to 180 W they found higher electron number densities, while the electron temperatures remain same.

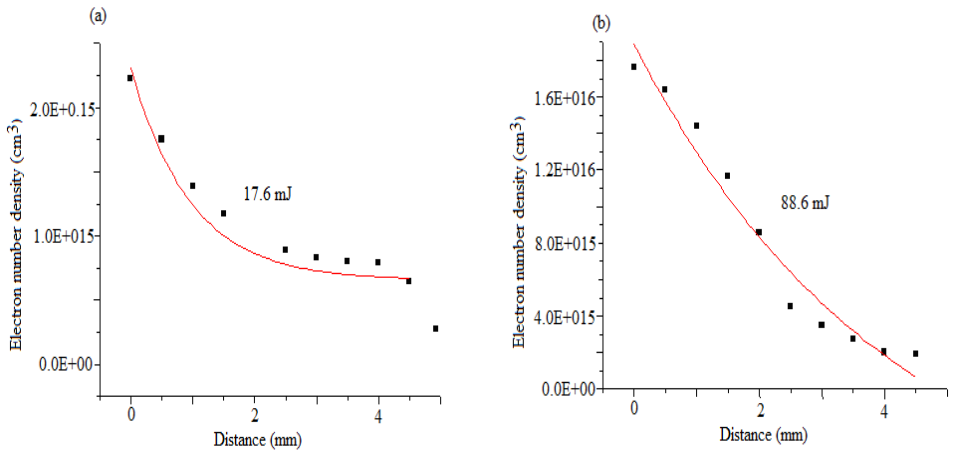

Fig 6: Effect on electron temperature and electron number density along the direction of propagation of the plume at 532 nm.

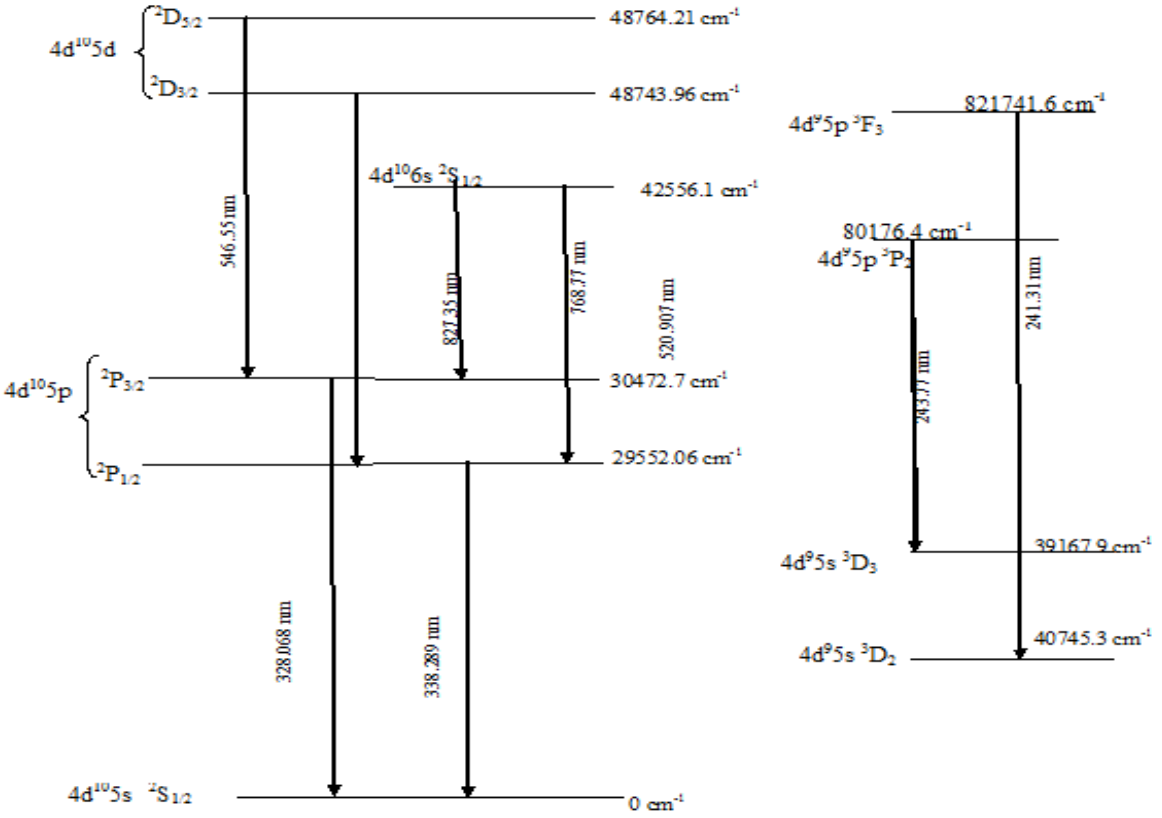

Fig. 7: Energy level diagram of neutral silver showing all the prominent transitions.

4 Conclusion

The effect of Q-switched Nd:YAG laser on Ag plasma ET, END and their behavior as a function of distance and energy along the direction of expansion path has been evaluated and results reveal that both ET and END decreases along the direction of expansion of the plasma and the mass ablation rate is at a maximum for the higher incident energy. Furthermore, the relationship of END and ET is directly related to laser irradiation and inverse to the distance laser beam source of target surface.

Acknowledgements

The authors are thankful to Higher Education Commission (HEC) of Pakistan for providing laser spectroscopy equipment and Dr. Nek Muhammad Shaikh, Q. A. University, Islamabad, for technical assistance during the research work.

References

[1] M.M. Krupa, A.N. Pogorily, L.L. Sartinska, Yu.V. Skirta, R. Zaharov, “Formation of the nanodots and change of the characteristics of thin magnetic films under laser irradiation”, Current Appl Phys, Vol. 10, pp. 294-298 (2010).

[2] S.B. Mansour, B.S. Yilbas, “Laser short-pulse heating of silicon film with the presence of metallic substrate”, Current Appl Phys, Vol. 10, pp. 1243-1248 (2010).

[3] S.M. Pawar, A.V. Moholkar, I.K. Kim, S.W. Shin, J.H. Moon, J.I. Rhee, J.H. Kim, “Effect of laser incident energy on the structural, morphological and optical properties of Cu2ZnSnS4 (CZTS) thin films”, Current Appl Phys, Vol. 10, pp. 565-569 (2010).

[4] B.I. Gornushkin, U. Panne, “Radiative models of laser-induced plasma and pump-probe diagnostics relevant to laser-induced breakdown spectroscopy”, Spectrochim Acta B, Vol. 65, pp. 345-359 (2010).

[5] E.A. Ershov-Pavlov, K.Yu. Katsalap, K.L. Stepanov, Yu.A. Stankevich, “Time-space distribution of laser-induced plasma parameters and its influence on emission spectra of the laser plumes”, Spectrochim Acta B, Vol. 63, pp. 1024-1037 (2008).

[6] Q.L. Ma, V. Motto-Ros, W.Q. Lei, M. Boueri, X.S. Bai, L.J. Zheng, H.P. Zeng, J. Yu, "Temporal and spatial dynamics of laser-induced aluminum plasma in argon background at atmospheric pressure: Interplay with the ambient gas", Spectrochim Acta B, Vol. 65, pp. 896–907 (2010).

[7] C.A. Henry, P.K. Diwakar, D.W. Hahn, "Investigation of helium addition for laser-induced plasma spectroscopy of pure gas phase systems: Analyte interactions and signal enhancement", Spectrochim Acta B, Vol. 62, pp. 1390-1398 (2007).

[8] V.I. Babushok, F.C. DeLucia Jr, J.L. Gottfried, C.A. Munson, A.W. Miziolek, "Double pulse laser ablation and plasma: Laser induced breakdown spectroscopy signal enhancement", Spectrochim Acta B, Vol. 61, pp. 999-1014 (2006).

[9] J.J. Camacho, L. Díaz, M. Santos, J.M.L. Poyato, "Time-resolved optical emission spectroscopic measurements of He plasma induced by a high-power CO2 pulsed laser", Spectrochim Acta B, Vol. 66, pp. 57-66 (2011).

[10] A. De Giacomo, M. Dell'Aglio, A. Santagata, R. Teghil, "Early stage emission spectroscopy study of metallic titanium plasma induced in air by femtosecond and nanosecond-laser pulses", Spectrochim Acta B, Vol. 60, pp. 935-947 (2005).

[11] E.S. Simpson, G.A. Lithgow, S.G. Buckley, "Three-dimensional distribution of signal from single monodisperse aerosol particles in laser induced plasma: Initial measurements", Spectrochim Acta B, Vol. 62, pp. 1460-1465 (2007).

[12] P. Stavropoulos, C. Palagas, G.N. Angelopoulos, D.N. Papamantellos, S. Couris, "Calibration Measurements in laser-induced breakdown spectroscopy using nanosecond and picosecond lasers", Spectrochim Acta B, Vol. 59, pp. 1885 (2004).

[13] C. Aragón, J.A. Aguilera, "Characterization of laser induced plasmas by optical emission spectroscopy, a review of experiments and methods", Spectrochim Acta B, Vol. 63, pp. 893-916 (2008).

[14] N.M. Shaikh, B. Rashid, S. Hafeez, Y. Jamil, M.A. Baig, "Measurement of electron density and temperature of a laser-induced zinc plasma", J Phys D Appl Phys, Vol. 39, pp. 1384-1391 (2006).

[15] A.W. Miziolek, V. Pallesschi, I. Schecchter, "Laser-induced breakdown spectroscopy", Cambridge University Press, Cambridge (2006).

[16] D.A. Cremers, L.J. Radziemski, "Handbook of laser-induced breakdown spectroscopy", John Wiley & Sons Ltd, West Sussex (2006).

[17] D. Böker, D. Brüggemann, "Temperature measurements in a decaying laser-induced plasma in air at elevated pressures", Spectrochim Acta B, Vol. 66, pp. 28-38 (2011).

[18] X.L. Mao, W.T. Chan, M. Caetano, M.A. Shannon and R.E. Russo, "Preferential vaporization and plasma shielding during nano-second laser ablation", Appl Surface Sci, Vol. 96, pp. 126-130 (1996).

[19] W. Pietsch, B. Dubreuil and A. Briand, "A study of laser-produced copper plasma at reduced pressure for spectroscopic applications", Appl Phys B, Vol. 61, pp. 267 (1995).

[20] D.N. Stratis, K.L. Eland, J.C. Carter, S.J. Tomlinson, S. M Angel, "Comparison of acousto-optic and liquid crystal tunable filters for Laser-Induced breakdown spectroscopy", Appl Spectro, Vol. 55, pp. 999-1004 (2001).

[21] M.A. Hafez, M.A. Khedr, F.F. Elaksher, Y.E Gamal, "Characteristics of Cu plasma produced by a laser interaction with a solid target", Plasma Source Sci Technol, Vol. 12, pp. 185 (2003).

[22] C. Aragón, J.A. Aguilera, "Determination of the local electron number density in laser-induced plasmas by Stark-broadened profiles of spectral lines Comparative results from Hα, Fe I and Si II lines", Spectrochim Acta B, Vol. 65, pp. 395-400 (2010).

[23] K.A. Bhatti, M. Khaleeq-ur-Rahman, M.S. Rafique, K.T. Chaudhary, A. Latif, "Electrons emission from laser induced metallic plasmas", Vacuum, Vol. 84, pp. 980-985 (2010).

[24] J.M. Gomba, C. D'Angelo, D. Bertuccelli, G. Bertuccelli, "Spectroscopic characterization of laser induced breakdown in aluminium lithium alloy samples for quantitative determination of traces", Spectrochim Acta B, Vol. 56, pp. 695-705 (2001).

[25] C. Prokisch, A.M. Bilgic, E. Voges, J.A.C. Broekaert, J. Jonkers, M. Van Sande, J.A.M. Van der Mullen, "Photographic plasma images and electron number density as well as electron temperature mappings of a plasma sustained with a modified argon microwave plasma torch MPT/measured by spatially resolved Thomson scattering", Spectrochim Acta B, Vol. 54, pp. 1253-1266 (1999).

[26] G. Abdellatif, H. Imam, "A study of the laser plasma parameters at different laser wavelengths", Spectrochim Acta B, Vol. 57, pp. 1155-1165 (2002).

[27] C. Aragon, J. Bengoechea, J.A. Aguilera, "Influence of the optical depth on spectral line emission from laser-induced plasmas", Spectrochim. Acta B, Vol. 56, pp. 619-628 (2001).

[28] J.A. Aguilera, C. Aragón, "Tempreture and electron density distribution of laser induced plasma generated with iron samples at different ambient gas pressure", Appl surface Sci, Vol. 197-198, pp. 173-180 (2002).

[29] V.K. Unnikrishnan, K. Alti, V.B. Kartha, C. Santhosh, G.P. Gupta, B.M Suri, "Measurements of plasma temperature and electron density in laser-induced copper plasma by time-resolved spectroscopy of neutral atom and ion emissions", Pramana J phys, Vol. 74, pp. 983-993 (2010).

[30] C-Y Ho, Y-H Tsai, Cheng-Sao Chen, Mao-Yu Wen, "Ablation of aluminum oxide ceramics using femtosecond laser with multiple pulses", Current Appl Phys, 1-5 (2011).

[31] A.M.E. Sherbini, H. Hegazy, T.M.E. Sherbini, "Measurement of electron density utilizing the Hα-line from laser produced plasma in air", Spectrochim Acta B, Vol. 61, pp. 532–539 (2006).

[32] H.R. Griem, "Principles of Plasma Spectroscopy", Cambridge Uni. Press, Cambridge (1997).

[33] J.R. Fuhr, W.L. Wiese, "NIST Atomic Transition Probability Tables, CRC Handbook of Chemistry & Physics", 7th Edition, D. R. Lide, Ed., CRC Press, Inc., Boca Raton (1996).

[34] B. Rashid, S. Hafeez, N.M. Shaikh, M. Saleem, R. Ali, M.A. Baig, "Diagnostics of copper plasma produced by the fundamental, second and third harmonic of a ND:YAG laser", Int J Modern Phys, Vol. B 21, pp. 2697-2710 (2007).

[35] M. Ying, Y. Xia, Y Sun, M Zhao, Y Ma, X Liu, Y Li, X. Hou, "Plasma properties of a laser-ablated aluminum target in air", Laser Particle Beams, Vol. 21, pp. 97-101 (2003).

[36] H. Lindner, K.H. Loper, D.W. Hahn, K. Niemax, "The influence of laser-particle interaction in laser induced breakdown spectroscopy and laser ablation inductively coupled plasma spectrometry", Spectrochim Acta B, Vol. 66, pp. 179-185 (2011).

[37] Y. Lu, Z. Tao, M. Hong, "Characteristics of excimer laser induced plasma from an aluminum target by spectroscopic study", J Jpn Appl Phys, Vol. 38, pp. 2958-2963 (1999).

[38] M. Ying, Y. Xia, Y Sun, M Zhao, Y Ma, X Liu, Y Li, X. Hou, "Plasma properties of a laser-ablated aluminum target in air", Laser Particle Beams, Vol. 21, pp. 97-101 (2003).

[39] D. Gunther, S.E. Jackson, H.P. Longerich, "Laser ablation and arc/spark solid sample introduction into inductively coupled plasma mass spectrometers", Spectrochim Acta B, Vol. 54, pp. 381-409 (1999).

[40] A. Bogaerts, Z. Chen, "Effect of laser parameters on laser ablation and laser-induced plasma formation: A numerical modeling investigation", Spectrochim Acta B, Vol. 60, pp. 1280-1307 (2005).

[41] L. Wu, R. Shen, J. Xu, Y. Ye, Y. Hu, "Spectroscopic study of laser-induced cu plasma with and without the confinement of a substrate", IEEE Transactions on Plasma Sci, Vol. 38, pp. 174-180 (2010).